Research Article

Jinguang Zhang, Yang Huang, Xiangyu Ma, Xianglong Wen*, Jun Rao, Yukuan Dou and Meng Zang

Effects of layup parameters and interference value on the performance of CFRP-metal interference fit joints

https://doi.org/10.1515/secm-2022-0016 received February 14, 2022; accepted May 16, 2022

Abstract: Based on the thick-wall cylinder theory and composite material mechanics, the stress distribution model of the CFRP shaft tube and metal shaft head has been established, and the relationship between the layup parameters and the value of interference on the maximum assembly force and failure torque in the interference fit joints of the CFRP shaft tube and the metal shaft head is deduced. Combining the three-dimensional finite element analysis model with experimental data, the result shows that the layup angles of the CFRP shaft tube have a greater influence on the joint connection performance than the layup sequence, and the larger the layup angle, the better the joint assembly performance while keeping the value of interference constant. The maximum assembly force and failure torque of the interference fit joints increase linearly while the value of the interference amount increases when the layup parameters are constant.

Keywords: interference fit, layup parameters, interference value, maximum assembly force, failure torque

ORCID: Jinguang Zhang 0000-0002-2503-1474; Xianglong Wen 0000-0003-1574-2384

1 Introduction

CFRP has been widely used in industrial applications owing to its high-performance properties, such as impact resistance, high-temperature resistance, and good repairability [1]. Composite-to-metal joining has become an essential technology in the assembly of many engineered structures [2]. Interference fit joints is a method of joint that maintains mechanical structure through interference between materials, and it is the most efficient in reducing weight as it requires no fasteners or additives and provides a mechanically reliable retention mechanism, particularly for joining concentric members [3]. The interference fit can improve the joint stiffness per unit of the accepted area [4,5]. Therefore, it is of great significance to study the performance of the interference fit joints.

So far, many researchers have already conducted theoretical derivations and experimental analyses of metal-to-metal interference fit joints, and many research results have been obtained [6]. Many parameters of interference fit joints for metal-to-metal have been studied, including the effects of a percentage interference fit, distribution of stresses around the interference fit fasteners [7–11], dynamic characteristics of interference fit joints [12], damage caused by the interference fit fasteners, etc. [13,14].

Compared to metal-metal jointing, there are few studies about composite-metal jointing [2]. The stress-strain of composite-metal joining is more complicated when they are subjected to interference assembly loads and torsional loads. Studies about composite-metal jointing connected using interference fit pins, interference fit bolts, and interference fit fasteners have been performed using finite element modeling and experimental testing [15,16]. The effect of the percentage of interference, the stress distribution and the analysis of the damage mechanism have also been achieved partially [17–22]. Raju et al. found that the load sharing of joints with interference fit was 10% higher than that of joints with the neat fit but limited to

^{*} Corresponding author: Xianglong Wen, School of Mechanical and Electronic Engineering, Wuhan University of Technology, Wuhan, China; Hubei Provincial Engineering Technology Research Center for Magnetic Suspension, Wuhan, China, e-mail: wenxl@whut.edu.cn Jinguang Zhang: School of Mechanical and Electronic Engineering, Wuhan University of Technology, Wuhan, China; Institute of Advanced Material and Manufacturing Technology, Wuhan University of Technology, Wuhan, China

Yang Huang, Xiangyu Ma, Jun Rao, Yukuan Dou, Meng Zang: School of Mechanical and Electronic Engineering, Wuhan University of Technology, Wuhan, China

a certain value of interference by FEA modeling [23]. Kaifu Zhang et al. found that the orientation of the fiber filaments has a strong influence on the frictional properties of the material surface by studying the micro-motor behavior of the interface between CFRP and titanium alloy [27].

There are few studies about the stress distribution, damage failure, and torsional performance in the process of interference value assembly and torsion of interference fit joints subjected to torsional loads. In this article, the interference fit joints between the CFRP shaft tube and the metal shaft head are taken as the research object, focusing on the relationship among layup parameters, interference value, and maximum assembly force and failure torque. First, the effects of layup parameters and interference value on the maximum assembly force and failure torque are deduced. The effect of the interference fit joints on maximum assembly and failure torque of joints is determined under the layup parameters and interference value using experimental tests and FEA modeling.

2 Analytical model

In engineering structures, a wall thickness to diameter ratio greater than or equal to 1/20 of cylindrical structures is considered thick-wall cylinders. When subjected to uniform internal or external pressure to the thick-wall cylinders, the stress along the wall thickness direction is non-uniform, and the torque is symmetrical about the axis of rotation.

Figure 1 shows a thick-wall cylinder structure with inner and outer diameters R_a and R_b , respectively. The inner and outer walls of the cylinder are subjected to internal pressure q_i and external pressure q_o , respectively.

Interference fit joints consisting of metal shaft and CFRP tube is shown in Figures 2 and 3. According to the thick wall cylinder analysis in elastic–plastic mechanics, the radial displacement at any point inside the cylinder is as follows [24]:

$$u = \frac{1 - v}{E} \frac{R_a^2 q_i - R_b^2 q_o}{R_b^2 - R_a^2} \times r + \frac{1 + v}{E} \frac{R_a^2 R_b^2 (q_i - q_o)}{R_b^2 - R_a^2} \times \frac{1}{r}.$$
 (1)

The interference fit joints between the CFRP shaft tube and the metal shaft head are characterized in macromechanics as a static friction behavior. When the interference fit joints are assembled, the contact surface stress caused by assembly deformation will generate static friction torque on the cylinder surface. The interference fit joints failure is invalid when the applied torque is greater than the static friction torque.

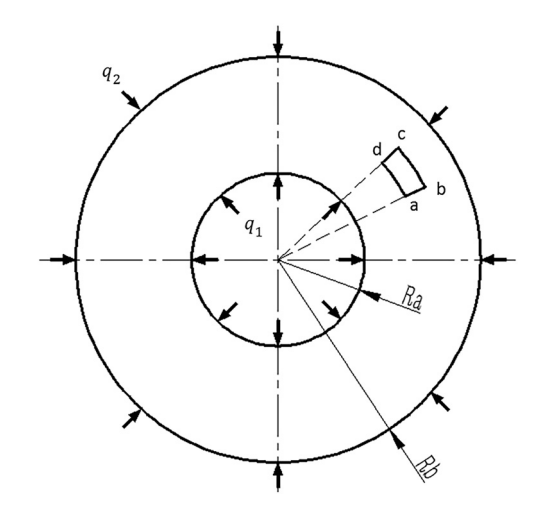


Figure 1: Schematic diagram of the thick-wall cylinder.

When the interference fit joints is only subjected to torque, the frictional resistance moment generated on the mating surface is greater than or equal to the torque for the joints not to be damaged. The relationship between the maximum assembly force, failure torque and contact surface stress, and other relevant parameters at this point can be described as follows:

$$F = \sigma_c f \pi dl, \tag{2}$$

$$M = \frac{\sigma_c f \pi d^2 l}{2}.$$
 (3)

In combination with equation (1), the minimum interference value between the CFRP shaft tube and the metal shaft head in the assembly process in the interference fit joints can be obtained. The influence of the pressing depth of the CFRP shaft tube and the metal shaft head on the performance of interference fit joints should be taken into

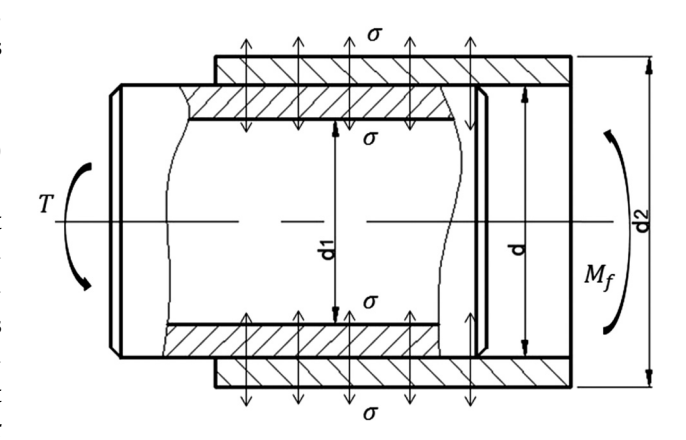


Figure 2: Geometry of the interference fit joints.

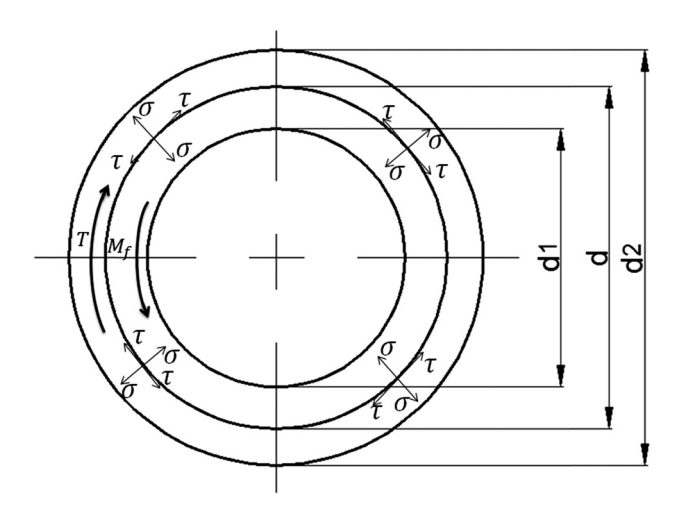


Figure 3: Cross-section of interference fit joints.

account when a pressing method is used for assembling [25].

$$\delta_{\min} = 2|e_m| + 2|e_f| + S_m + S_f,$$
 (4)

where S_m and S_m are the pressing depth of the CFRP shaft tube and the metal shaft head, respectively. When $S_m = 1.6R_{am}$ and $S_m = 1.6R_{af}$, $M \ge T$, the constitutive equation can be written as follows:

$$F = \frac{(\delta_{\min} - 1.6R_{am} - 1.6R_{af})\pi d^{2}lf}{\frac{d_{mo}^{2}}{E_{m}} \left(\frac{d_{mo}^{2} + d_{mi}^{2}}{d_{mo}^{2} - d_{mi}^{2}} - v_{1}\right) + \frac{d_{mo}^{2}}{E_{f\theta}} \left(\frac{d_{mo}^{2} + d_{fo}^{2}}{d_{fo}^{2} - d_{mo}^{2}} + v_{fr\theta}\right)},$$
(5)

$$M = \frac{(\delta_{\min} - 1.6R_{am} - 1.6R_{af})\pi d^{2}lf}{\frac{2d_{mo}}{E_{m}} \left(\frac{d_{mo}^{2} + d_{mi}^{2}}{d_{mo}^{2} - d_{mi}^{2}} - \nu_{1}\right) + \frac{2d_{mo}}{E_{f\theta}} \left(\frac{d_{mo}^{2} + d_{fo}^{2}}{d_{fo}^{2} - d_{mo}^{2}} + \nu_{fr\theta}\right)}.$$
 (6)

As shown in equations (5) and (6), Young's modulus, interference value, and coefficient of friction of the CFRP shaft tube and the metal shaft head have a significant effect on the maximum assembly force and failure torque of interference fit joints. For the CFRP shaft tube, the circumferential modulus can be changed by changing the composite layups. The larger the $E_{f\theta}$, the smaller the denominator, and the larger the value for the fractional expression of the maximum assembly force and the failure torque, the better the connection performance of the interference fit joints. On the contrary, the smaller the circumferential modulus of elasticity of the CFRP shaft tube, the worse the joint performance of the interference joints. While the interference value changes in the equation, the greater the interference, the greater the maximum assembly force and failure torque of the interference fit joints, and the better the performance of the interference fit joints.

The calculation of the circumferential modulus of the CFRP shaft tubes can be derived from the classical laminate theory of CFRP [26]. The composite laminated structure consists of a single layer of material stacked in the thickness direction, and the stress–strain expressions under the action of neutral surface strain and curvature are as follows:

$$\begin{bmatrix} \sigma_{11} \\ \sigma_{22} \\ \sigma_{12} \end{bmatrix} = \frac{1}{h} [A] \begin{bmatrix} \varepsilon_{11}^{0} \\ \varepsilon_{22}^{0} \\ \gamma_{12}^{0} \end{bmatrix} + \frac{1}{h} [B] \begin{bmatrix} k_{12} \\ k_{22} \\ k_{12} \end{bmatrix}, \tag{7}$$

where 1 is the fiber orientation, 2 is the direction perpendicular to the fiber orientation (the circumferential direction of CFRP shaft tube in this article), and 3 is the thickness direction. ε_{11}^0 , ε_{22}^0 , and γ_{12}^0 are the neutral surface line strain and shear strain, respectively. k_{12} , k_{22} , and k_{12} are the neutral surface deflection rate and twist rate, respectively, [A] and [B] denote the tensile stiffness matrix and the coupling stiffness matrix. The subterms in the matrix are as follows:

$$\begin{cases}
A_{mn} = \sum_{j=1}^{N} (\bar{Q}_{mn})_{j} (h_{j} - h_{j-1}), \\
B_{mn} = \frac{1}{2} \sum_{j=1}^{N} (\bar{Q}_{mn})_{j} (h_{j}^{2} - h_{j-1}^{2}),
\end{cases} (8)$$

where h_j is the distance from the bottom of the jth layer to the neutral plane.

In a CFRP structure with a symmetrical layup, the coupling matrix [B] = 0. The combined strain–stress relationship can be described as follows:

$$\sigma_{11} = \frac{E_1}{1 - v_{12}v_{21}} \varepsilon_{11} + \frac{v_{21}E_2}{1 - v_{12}v_{21}} \varepsilon_{22}.$$
 (9)

The circumferential modulus of the CFRP shaft tube could be obtained as:

$$E_{2} = \frac{\left[\sum_{N}^{j=1} (\bar{Q}_{22})_{j} (h_{j} - h_{j-1})\right] \left[\sum_{N}^{j=1} (\bar{Q}_{11})_{j} (h_{j} - h_{j-1})\right] - \left[\sum_{N}^{j=1} (\bar{Q}_{12})_{j} (h_{j} - h_{j-1})\right]^{2}}{\left[\sum_{N}^{j=1} (\bar{Q}_{11})_{j} (h_{j} - h_{j-1})\right]},$$
(10)

where \bar{Q}_{11} , \bar{Q}_{12} , and \bar{Q}_{22} are the subterms of the stiffness transposed matrix $[\bar{Q}]$.

For a CFRP structure with an asymmetric layup, the single-layer circumferential modulus is as follows:

$$E_{y\theta} = \frac{1}{\bar{S}_{22}} = \frac{1}{S_{22}(\sin^4\theta + \cos^4\theta) + (S_{11} + S_{22} - S_{66})\sin^2\theta\cos^2\theta},$$
 (11)

where S_{11} , S_{22} , and S_{66} are the subterms of the flexibility matrix [S].

The circumferential modulus of the laminated structure is as follows:

$$E_{\theta} = \sum [(E_{y\theta})V_{\theta}], \tag{12}$$

where $E_{y\theta}$ is the circumferential modulus of the singlelayer fiber corresponding to a layup angle of θ , and V_{θ} is the ratio of the angle to the thickness direction.

Based on the above equation, it can be found that changing the layup parameters of the CFRP shaft tubes will affect the circumferential modulus, which will lead to changes in the maximum assembly force and failure torque of the interference fit joints.

3 FEA model

3.1 FEA model of interference fit joints

As shown in Figure 4, the interference fit joints consist of a metal shaft head and a CFRP shaft tube. The material of the metal shaft head is 45# steel with the properties as shown in Table 1. The CFRP shaft tube material is T700/8002 prepreg, and the performance parameters, as shown in Table 2, are provided by Zhongfu Shenying Carbon Fiber Co., Ltd, and the number of layups is 20 in the simulation. The dimensional parameters of interference fit joints are given in Table 3.

The FEA model of the interference fit joints is built-in ABAQUS according to the parameters in Table 3. The CFRP shaft tube layup sequence is from inside to outside. Considering that the process of interference fit produces significant geometric changes, it is necessary to turn on

Table 1: Mechanical properties of 45 steel

Elastic modulus E (GPa)	Poisson's ratio v	Shear strength τ (MPa)
210	0.263	175

Table 2: Unidirectional composite properties (T700/8002)

Properties	Values	Properties	Values
<i>E</i> ₁ (GPa)	150	G ₁₃ (GPa)	5.12
E_2 (GPa)	9	G_{23} (GPa)	3.34
E_3 (GPa)	9	X_{t} (MPa)	2,350
<i>V</i> ₁₂	0.24	Y_{t} (MPa)	86
V ₁₃	0.24	X_{c} (MPa)	1,570
V ₂₃	0.28	Y_{c} (MPa)	340
G ₁₂ (GPa)	5.12	S ₁₂ (MPa)	104

the NIgeom in the step. The friction coefficient of penalty between the metal shaft head and the CFRP shaft tube is set to 0.1 when setting up interaction [27]. A surface-to-surface relative constraint should be added between the cylindrical structures. In the load, the end face of the metal shaft head away from the CFRP shaft tube is fully constrained, and the end facing away from the metal shaft head in the CFRP shaft tube is displaced 95 mm axially toward the end of the metal shaft head. Such a boundary condition setting is consistent with the experiments being conducted on the electronic testing machine. The C3D10 element and the SC8R element are applied to the metal shaft head and the CFRP shaft tube, respectively. The FEA model of the interference fit joint is shown in Figure 5. Referring to the principle of the mesh density

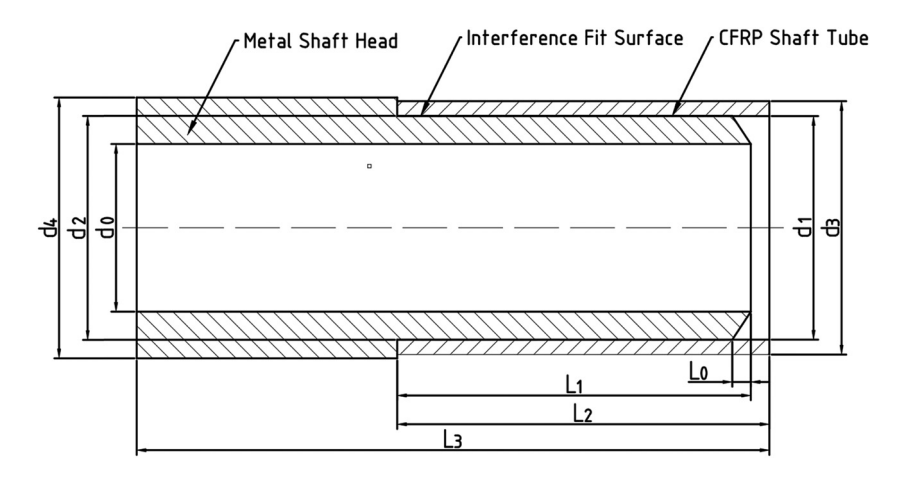


Figure 4: Schematic diagram of the interference fit joints.

Table 3: Shape size used in FEA model

Component		Length (mm)				diamet	er (mr	n)	
	Lo	L ₁	L ₂	L ₃	do	d ₁	d ₂	d ₃	d ₄
Data	5	95	100	165	45	60	60.1	68	70

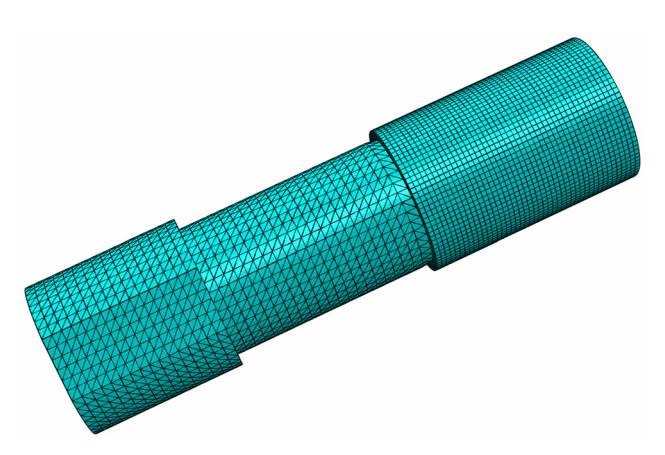


Figure 5: FEA model of interference fit joint.

for contacting the master and slave surfaces, the mesh size of the metal shaft head is twice as large as the CFRP shaft tube. Considering that the mesh size will directly affect the efficiency and accuracy of the finite element simulation, a sensitivity analysis is performed on the mesh of the FEA model. The average value of CPRESS in the output path of the contact surface is set as the evaluation criterion in Figure 6. Keeping the multiplicative relationship of the mesh settings, the result is shown in Figure 7. In order to have a good calculation efficiency and analysis accuracy, the mesh size of the metal shaft head is set as 4.5 mm.

The failure analysis of interference fit joints should be discussed separately considering that the joint consists of two materials. For the metal shaft head, 45# steel is the isotropic material and can be judged directly by the maximum Mises stress generated during assembly and

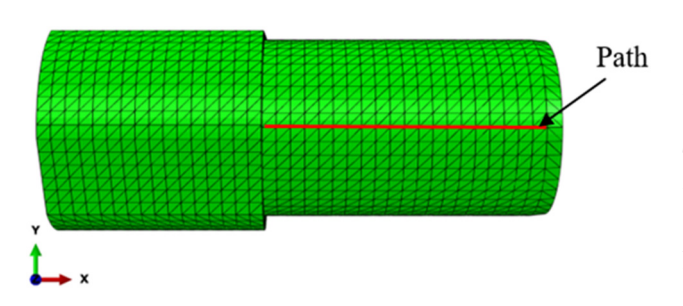


Figure 6: The path for contact surface stress output.

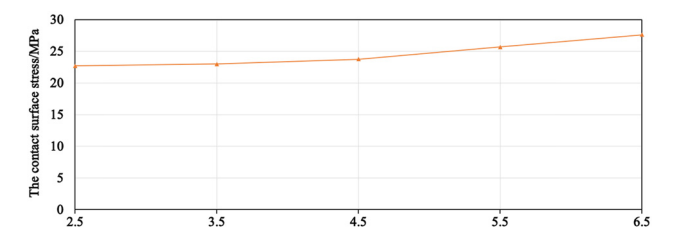


Figure 7: Element size sensitivity analysis.

torsion to determine whether failure occurs. When the maximum stress value is less than the fatigue failure strength of 45# steel 355 MPa, the metal shaft head does not fail. For the CFRP shaft tube, the material is anisotropic, and the Tsai-Wu criterion, which is the most common among the failure criteria of composite materials, is selected as failure judgment in this article. The VUMT subroutine in ABAQUS is used to perform a customized three-dimensional failure criterion on the Tsai-Wu criterion, which considers that failure occurs when the Tsai-Wu failure index FI is greater than or equal to 1. And the full expressions for the failure index are as follows:

$$FI = F_1\sigma_1 + F_2\sigma_2 + F_3\sigma_3 + F_{11}\sigma_1^2 + F_{22}\sigma_2^2 + F_{33}\sigma_3^2 + F_{44}\sigma_4^2 + F_{55}\sigma_5^2 + F_{66}\sigma_6^2 + 2F_{12}\sigma_1\sigma_2 + 2F_{13}\sigma_1\sigma_3 + 2F_{23}\sigma_2\sigma_3,$$
(13)

where
$$F_1 = \frac{1}{S_1^t} + \frac{1}{S_1^c}$$
, $F_2 = \frac{1}{S_2^t} + \frac{1}{S_2^c}$, $F_3 = \frac{1}{S_3^t} + \frac{1}{S_3^c}$, $F_{11} = -\frac{1}{S_1^t S_1^c}$, $F_{12} = -\frac{1}{S_2^t S_2^c}$, $F_{23} = -\frac{1}{S_2^t S_2^c}$, $F_{33} = -\frac{1}{S_2^t S_3^c}$, $F_{44} = \frac{1}{S_4^2}$, $F_{55} = \frac{1}{S_2^2}$, $F_{66} = \frac{1}{S_2^c}$, $F_{12} = -\frac{\sqrt{F_{11}F_{22}}}{2}$, $F_{13} = -\frac{\sqrt{F_{11}F_{33}}}{2}$, $F_{23} = -\frac{\sqrt{F_{22}F_{33}}}{2}$.

 σ_1 , σ_2 , σ_3 , σ_4 , σ_5 , and σ_6 are the normal stress in directions 1, 2, and 3 and the shear stress in planes 2–3, 1–3, and 1–2, respectively. S_1^t , ..., S_2^t , S_2^c , S_3^t , and S_3^c are the tensile strength and compressive strength of the materials in directions 1, 2, and 3, respectively. S_4 , S_5 , and S_6 are the shear strength of materials 2–3, 1–3, and 1–2 planes, respectively.

3.2 Effect of layup parameters on the performance of interference fit joints

3.2.1 Layup angles

The interference value is kept at 0.1 mm, and the effect on the performance of interference fit joints is obtained by changing the layup angles. Ten simulation schemes of layup angles are as follows: $[\pm 45^{\circ}]_{10}$, $[\pm 50^{\circ}]_{10}$, $[\pm 55^{\circ}]_{10}$, $[\pm 60^{\circ}]_{10}$, $[\pm 65^{\circ}]_{10}$, $[\pm 70^{\circ}]_{10}$, $[\pm 75^{\circ}]_{10}$, $[\pm 85^{\circ}]_{10}$, and $[\pm 90^{\circ}]_{10}$. The CPRESS is the output in ABAQUS for

156 — Jinguang Zhang et al. DE GRUYTER

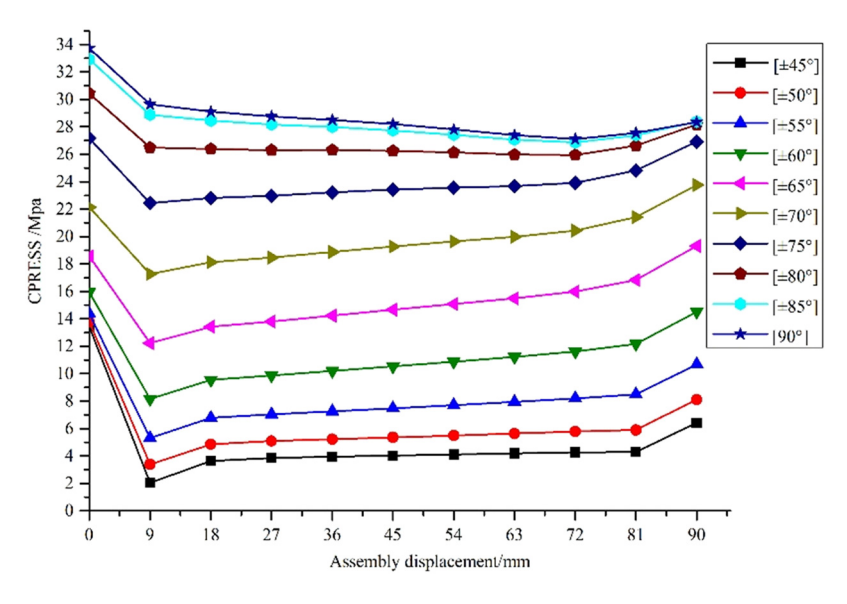


Figure 8: Distribution of contact surface stress values along the path at different angles.

contact surface stresses in interference fit joints. Figure 8 shows the distribution of CPRESS at different layup angles. Taking the average value of CPRESS, the maximum simulated assembly force and maximum failure torque can be calculated using equations (2) and (3).

As shown in Figure 8, the maximum CPRESS occurs when the laying angle is 90°, which indicates that it effectively improves the contact surface stress of the interference fit joints by increasing the layup angle. The maximum assembly force and failure torque increase with increasing layup angle provided that the metal shaft head and the CFRP shaft tube do not fail. Along the axial path of the surface, the maximum stress at the contact surface occurs at the beginning of the assembly due to the local stress concentration at the structural mutation. After contact occurs on the surface, the stress value on the contact surface increases gradually with the path. The maximum assembly force, the failure torque, the maximum stress on the metal shaft head during assembly, and torsion and the failure index of the CFRP shaft tube for the ten schemes are presented in Table 4. The maximum assembly force and the failure torque are plotted as shown in Figures 9 and 10.

As shown in Figures 9 and 10, the maximum assembly force and failure torque increase with the layup angles. The overall growth trend is slow-fast-slow. In Table 4, neither the metal shaft head nor the CFRP shaft tube has failed. However, when the layup angles increase, the failure index of the metal shaft head and the CFRP shaft tube also increases, which indicates that large layup angles can enhance the performance of interference fit joints, but

large layup angles also result in larger failure indices for the CFRP shaft tube.

3.2.2 Layup sequence

According to the theoretical prediction in Section 2, different layup sequences will also affect the mechanical properties of the CFRP shaft tube. The layup angles of $\pm 45^{\circ}$ and $\pm 80^{\circ}$ are selected to form five simulation schemes with different layering sequences as follows: $[\pm 45^{\circ}]_4[\pm 80^{\circ}]_6$, $[\pm 45^{\circ}]_2[\pm 80^{\circ}]_3[\pm 45^{\circ}]_2[\pm 80^{\circ}]_3$, $[\pm 80^{\circ}]_3[\pm 45^{\circ}]_2[\pm 80^{\circ}]_3[\pm 45^{\circ}]_2$, and $[\pm 45^{\circ}]_2[\pm 80^{\circ}]_6[\pm 45^{\circ}]_2$.

Table 4: Evaluation index of interference fit joints at different layup angles

Layup angles	Maximum assembly force (N)	Failure torque (N m)	Shaft head maximum stress (MPa)	Maximum failure index
[±45°] ₁₀	6,914	207.43	33.77	0.202
$[\pm 50^{o}]_{10}$	9,298	278.95	45.42	0.2071
[±55°] ₁₀	13,045	391.35	63.72	0.2241
$[\pm 60^{\circ}]_{10}$	18,445	553.36	90.1	0.2543
[±65°] ₁₀	25,635	769.06	125.2	0.2956
[±70°] ₁₀	33,468	1004.04	163.5	0.3416
[±75°] ₁₀	40,342	1210.25	197.1	0.3787
[±80°] ₁₀	44,884	1346.51	219.2	0.4023
[±85°] ₁₀	47,217	1416.52	230.6	0.4128
[±90°] ₁₀	47,907	1437.21	234	0.4151

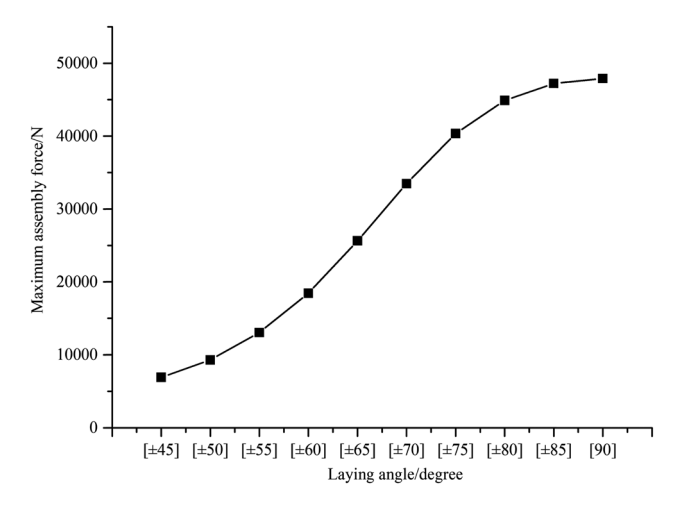


Figure 9: Relationship between maximum assembly force and laying angles.

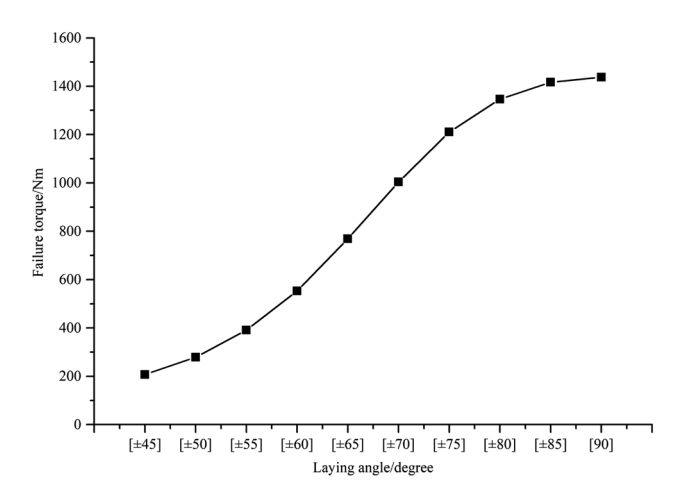


Figure 10: Relationship between failure torque and laying angles.

According to the analysis in the previous section, $\pm 80^{\circ}$ is chosen to ensure good performance of interference fit joints, and $\pm 45^{\circ}$ is chosen to ensure a certain safety margin for the joint components. The maximum assembly force, failure torque, maximum stress on the metal shaft head during assembly and torsion, and maximum failure index of the

CFRP shaft tube obtained from the simulation of the five layup sequences are shown in Table 5.

It can be seen from Table 4 that the maximum assembly force and failure torque change little when the layup sequences of the CFRP shaft tube change. The effect of layup sequences on maximum assembly force and failure torque is much less than that of layup angle. As far as the failure index of the CFRP shaft tube is concerned, the failure index of the CFRP shaft tube is small, when using small-angle layup and large-angle layup for the middle and outer layers of the CFRP shaft tube, respectively.

3.3 Interference value

In order to study the effect of different interference values on the performance of interference fit joints, five simulation schemes are designed. The layup parameter is $[\pm 75^{\circ}]_{10}$ and the interference values are 0.1, 0.08, 0.06, 0.04, and 0.02 mm, respectively. The distribution of CPRESS along the path as the value of interference changes is shown in Figure 11.

From Figure 11, it is seen that the value of CPRESS along the assembly path is first decreasing and then increasing. The maximum value occurs at the beginning of the assembly and is considered a stress concentration. Compared with Figure 8, it can be concluded that, without considering the stress concentration, the CPRESS will increase with the increase of the assembly displacement with the increase of either the layup angle or the interference value.

The maximum assembly force, the failure torque, the maximum stress on the metal shaft head during assembly and torsion, and the failure index of the CFRP shaft tube for the five scenarios are listed in Table 6. The influence of interference value changes the maximum assembly force and failure torque in schemes and are drawn as broken lines in Figures 12 and 13.

Table 5: Evaluation index of interference fit joints at different layup sequences

Layup sequences	Maximum assembly force (N)	Failure torque (N m)	Shaft head maximum stress (MPa)	Maximum failure index
[±45°] ₄ [±80°] ₆	31,187	935.62	92.58	0.3117
$[\pm 45^{\circ}]_{2}[\pm 80^{\circ}]_{3}[\pm 45^{\circ}]_{2}[\pm 80^{\circ}]_{3}$	31,271	938.12	88.91	0.2706
$[\pm 80^{\circ}]_{3}[\pm 45^{\circ}]_{4}[\pm 80^{\circ}]_{3}$	31,181	935.44	89.05	0.2684
$[\pm 80^{\circ}]_{3}[\pm 45^{\circ}]_{2}[\pm 80^{\circ}]_{3}[\pm 45^{\circ}]_{2}$	30,421	912.62	89.41	0.2978
$[\pm 45^{\circ}]_{2}[\pm 80^{\circ}]_{6}[\pm 45^{\circ}]_{2}$	30,667	920.02	89.4	0.3015

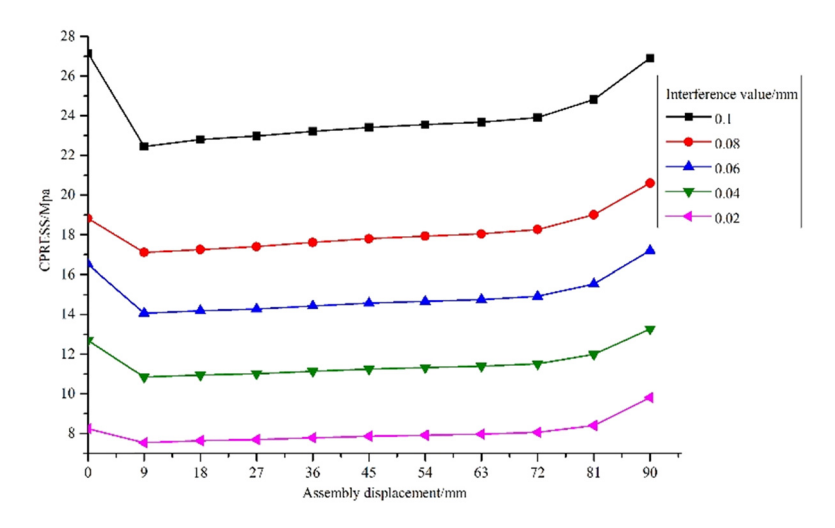
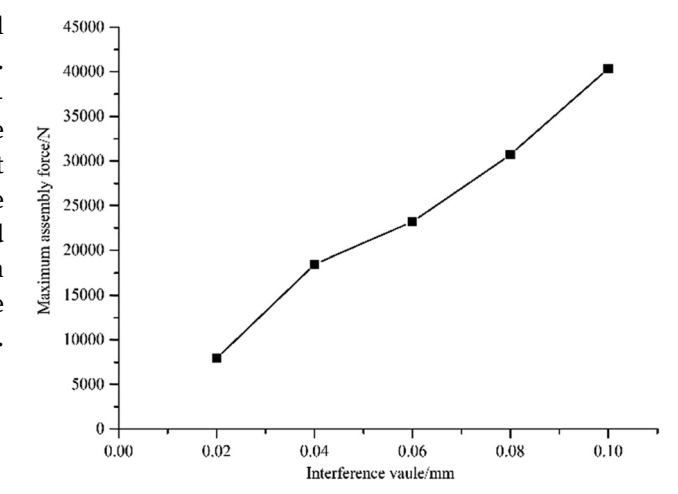


Figure 11: Distributions of CPRESS along the path at different interference values.

It can be seen from Table 6 that for both the metal shaft head and the CFRP shaft tube failure does not occur. The assembly force and the failure torque of the interference fit joints gradually increase with the increase of the interference value. Combined with Figures 12 and 13, it can be seen that the maximum assembly force and failure torque of the CFRP shaft tube and the metal shaft head interference fit joints are roughly linearly increasing with the value of interference, while the failure index of the CFRP shaft tube increases with the value of interference.



4 Experiment

4.1 Specimen preparation

In order to validate the results from the previous analyses, a set of assembly tests and torsional loading tests of the CFRP-metal interference fit joints are performed using the testing machine and the loading fixture. Five schemes of test samples are designed and determined based on the FEA model. As shown in Table 7, Schemes 1–3

Figure 12: Relationship between maximum assembly force and interference value.

investigate the effect of different layup angles on the assembly and torsion process of interference fit joints; Schemes 3–5 are designed to study the effects of different interference values on the assembly and torsion process of interference fit joints. It should be noted that the

Table 6: Evaluation index of interference fit joints at different interference values

Interference values (mm)	Maximum assembly force (N)	Failure torque (N m)	Shaft head maximum stress (MPa)	Maximum failure index
0.1	40,342	1,210.25	197.1	0.3787
0.08	30,708	921.23	145.9	0.3598
0.06	23,191	695.37	122.5	0.2932
0.04	18,436	553.08	95.7	0.2265
0.02	7,941	238	56.89	0.1598

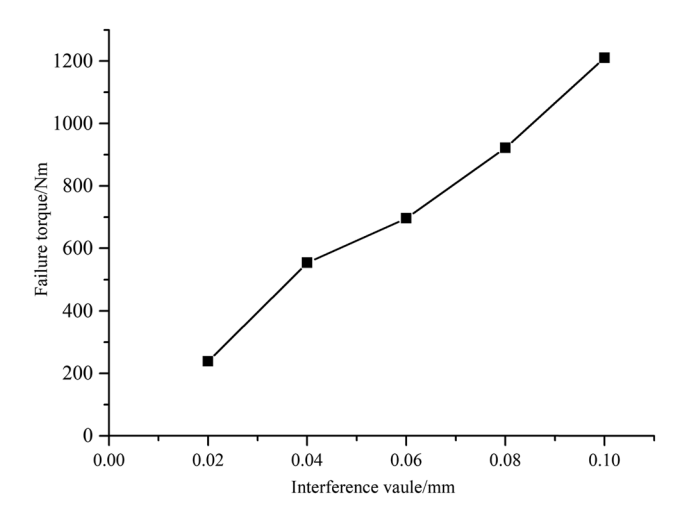


Figure 13: Relationship between failure torque and interference value.

Table 7: Schemes for interference fit joints

Scheme	Layup angles	Interference value (mm)	Specimen group
Scheme 1	[±45°] ₁₀	0.12	1,2
Scheme 2	$[\pm 60^{o}]_{10}$	0.12	3,4
Scheme 3	[±75°] ₁₀	0.12	5,6
Scheme 4	[±75°] ₁₀	0.08	7,8
Scheme 5	[±75°] ₁₀	0.04	9,10

interference value in this experiment is changed by machining different outer diameter sizes of the metal shaft heads. In order to consider the influence of surface roughness, size deviation, etc. on the interference value, the actual interference values of 0.12, 0.08, and 0.04 mm correspond to the interference values of 0.1, 0.06, and 0.02 mm in theoretical analysis.

The CFRP shaft tube is made by prepreg material coil technology. Roll-wrapping the T700/8002 prepreg over a precisely machined mandrel and then being cured through a curing oven, then the composite tube is machined to the required length. A thickness of 0.2 mm per ply of prepreg. The mandrel is machined by turning 45# steel, the tolerance of the outer dimension is ± 0.01 mm, and the surface roughness is R_a 6.3. The metal shaft head is CNC milled by 45# steel to ensure the dimension tolerance of ±0.01 mm and surface roughness of R_a 6.3. The mandrel and the metal shaft head are deburred after machining and then measured with the surface roughness measuring instrument to ensure that the roughness meets the requirements. The contact surface of interference fit joints is polished to the same surface roughness within R_a 6.3 using an abrasive finishing machine and thoroughly cleaned with ethanol in an ultrasonic bath for 10 min prior to experimental tests. Considering that the stacking sequence and manufacturing constraints in the fabrication of the composite material components severely affect the resultant properties [28,29], all the above manufacturing processes are completed by Zhongfu Shenying Carbon Fiber Co., Ltd, China.

4.2 Experimental study on assembly

Assembly test is performed using DNS-100 electronic testing machine. During the test, the metal shaft head is placed vertically on the compression table with the end to be assembled facing upward, the CFRP shaft tube is placed vertically in the stepped position at the end of the contact surface of the metal shaft head, and

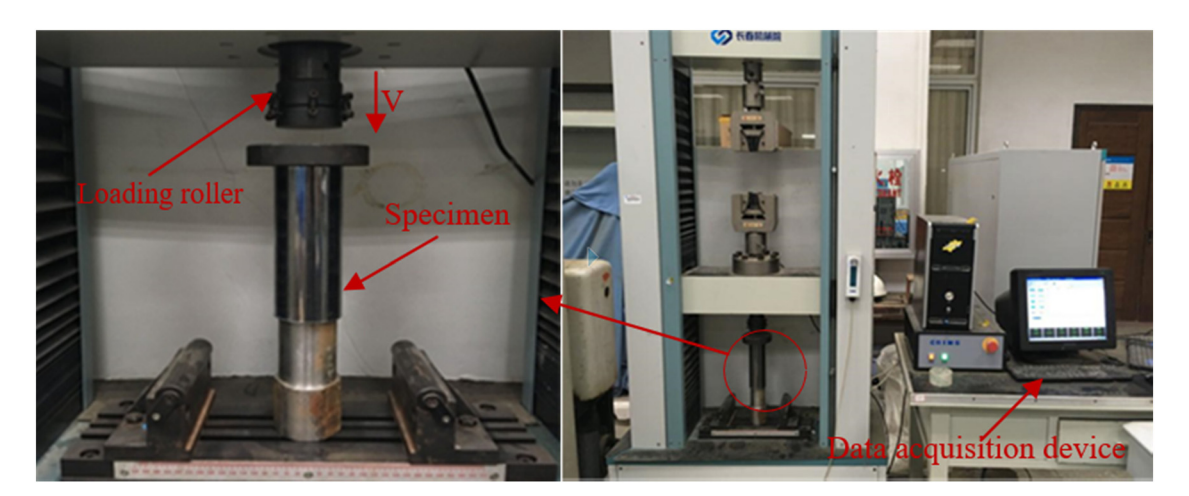


Figure 14: Interference fit joint assembly measurement platform.

160 — Jinguang Zhang et al.

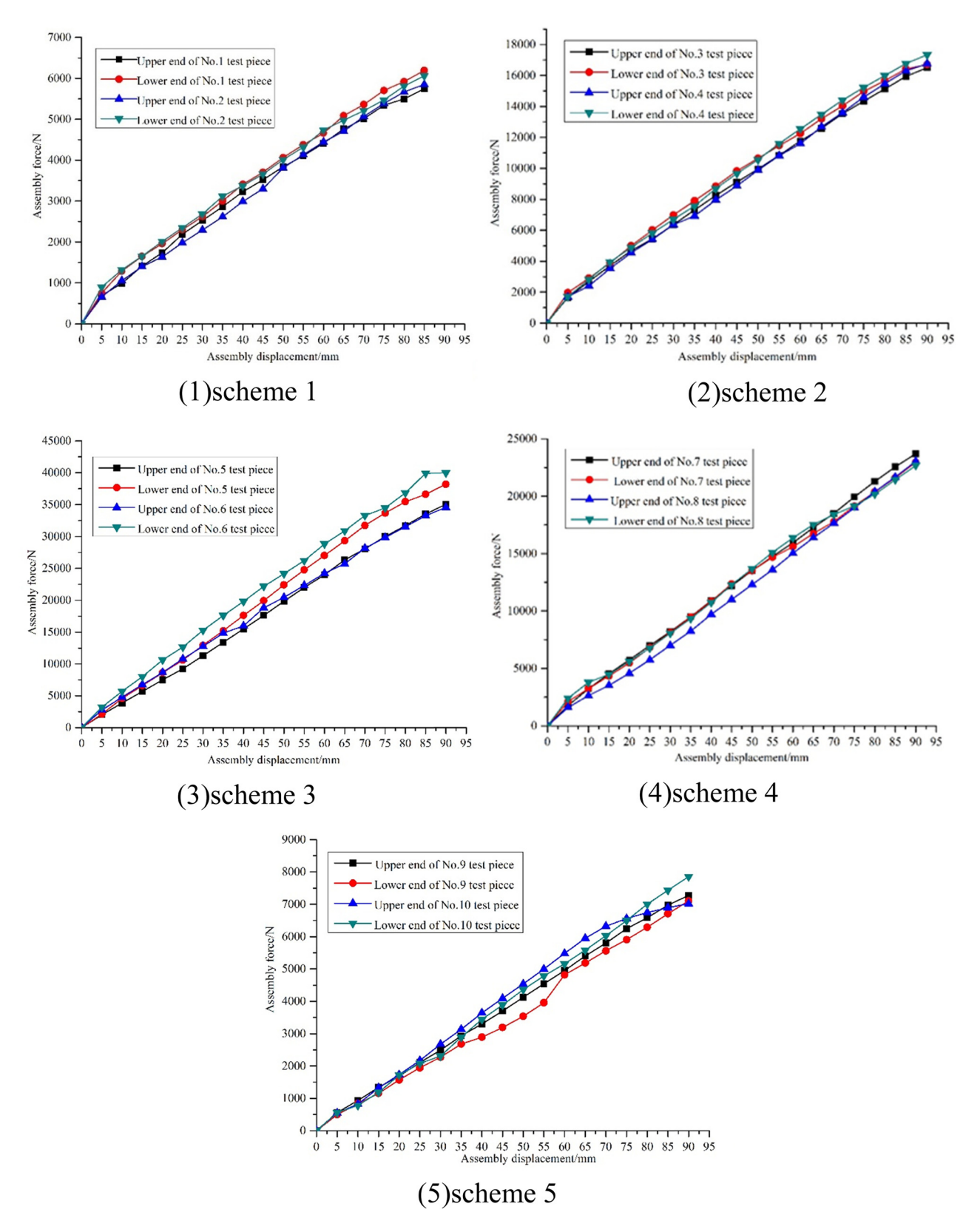


Figure 15: Assembly force-displacement relationship in different schemes.

Scheme	Specimen group	Analytical result (N)	FEA results (N)	Test results (N)
Scheme 1	1	6,661	6,914	Upper end: 6,086 lower end: 6,442
	2			Upper end: 6,109 lower end: 6,351
Scheme 2	3	17,451	18,445	Upper end: 16,503 lower end: 16,699
	4			Upper end: 16,753 lower end: 17,335
Scheme 3	5	37,333	40,342	Upper end: 35,049 lower end: 38,197
	6			Upper end: 34,555 lower end: 39,971
Scheme 4	7	22,400	23,191	Upper end: 23,701 lower end: 22,960
	8			Upper end: 23,041 lower end: 22,681
Scheme 5	9	7,467	7,941	Upper end: 7,271 lower end: 7,105
	10			Upper end: 7,018 lower end: 7,853

the flat pressure block is placed horizontally at the other end of the shaft tube as shown in Figure 14. The loading roller moves downward at a uniform speed of 5 mm/min.

In the assembly process, the assembly force increases linearly with the increase of assembly displacement. When the assembly displacement is 90 mm, the assembly force reaches the maximum value. The assembly force variation with displacement under different schemes for the interference fit joints is summarized in Figure 15. The FEA results and test results for each scheme are recorded in Table 8.

Figure 15 and Table 8 show that the assembly force increases at a faster rate when the displacement is 0-5 mm; the reason is the stress concentration generated in the assembly process at the step of the alignment. The maximum error arising from the theoretical and experimental results is 8% from scheme 3. The analysis may be due to defects such as the prepreg breaking the continuity of some fibers during the cutting process, bubbles, and micro-cracks during the molding process. The maximum error of 15.7% between the experimental parts comes from scheme 3, which may be caused by the machining error of the sample and the difference between the actual interference values during assembly.

Comparing schemes 1, 2, and 3, keeping the interference value constant, the larger the layup angle, the larger the maximum assembly force. It can be considered that the circumferential stiffness of the CFRP shaft tube

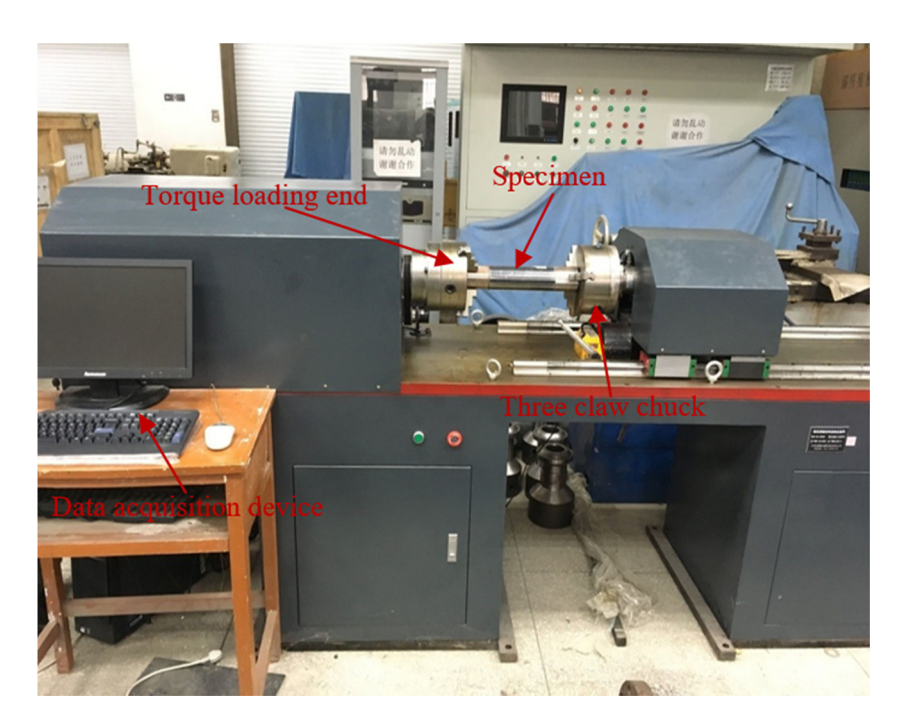


Figure 16: Interference fit joint torsion measurement platform.

Table 9: Sensitivity study on the failure torques under the interference fit joints

Scheme	Specimen group	Analytical result (N m)	FEA results (N m)	Test results (N m)
Scheme 1	1	199.82	207.43	202.5
	2			194.3
Scheme 2	3	523.54	553.36	454.4
	4			436.8
Scheme 3	5	1120	1210.25	992.4
	6			930.8
Scheme 4	7	672	695.37	673.4
	8			663
Scheme 5	9	224	238	210.5
	10			213.6

increases with the increase of the layup angle. Schemes 3, 4, and 5 show that the maximum assembly force decreases with decreasing interference value when keeping the layup parameters constant. The conclusions are mutually consistent with the prediction laws in Section 2.

4.3 Experimental study on torsion

A set of torsional loading tests of the interference fit joints are performed using the NZ-W2000 torsion tester and are shown in Figure 16. Before torsional loading, a line is drawn at the interference fit joints as a reference and the specimen is subsequently set up for an angular velocity control test at a speed of 0.05°/min. Recording the maximum value of the torque in the test, that is, the failure torque of the interference fit joints, and observing the misalignment of the scribing line to determine the first failure position of the bilateral interference fit joints. Figure 16 shows the joint specimen under the test.

During the torsion, the torque value increases gradually as the spindle is slowly loaded at a uniform speed. When the torque increases to a certain value and then suddenly decreases, the torque remains roughly constant at a certain value as the spindle continues to run. The above phenomenon is analyzed as the interference fit joints before failure, mainly by the interference surface generated by the static friction force to form the friction torque to resist the active torsional moment. When the active torsional moment is greater than the static friction moment, the interference fit joints part of the failure, at this time the active torsional moment is equal to the friction moment formed by the friction force, and with the spindle movement to maintain the same. The maximum

failure torque of different test parts are recorded. FEA results and test maximum torque values are recorded in Table 9.

As shown in Table 9, the joint torsional failure value is the largest of scheme 3, which indicates that scheme 3 is the best of the five interference fit joints options. The results of all five schemes show that the test results are lower than those predicted by the FEA model, reason is that there are structural differences and process defects in the fabrication and machining of the experimental parts. However, the trends of the results calculated by the three methods are consistent with each other. Analyzing the results of the data, the failure torque increases with the increase of the layup angle when keeping the interference value constant. Keeping the layup parameters constant, the failure torque increases with the increase in the value of interference, which is in agreement with the predictions in Section 2.

Observing the torsional failure area of each sample, No. 1, No. 2, No. 3, No. 5, No. 6, and No. 10 samples have upper flange twist failure, No. 7–9 samples have a torsional failure of the lower end flange, and No. 4 flange had a torsional failure of both end faces. Comparing the failure phenomena obtained from the test with the assembly forces in Table 8, it is found that the end with the smaller maximum assembly force of the different parts failed first in torsion, which justified the data collection.

5 Conclusions

In order to investigate the effect of layup parameters and interference value on the performance of CFRP-metal interference fit joints, an experimental study is carried out. Maximum assembly and failure torque are performed on five different CFRP-metal joint samples, namely interference fit joints. Some conclusions are obtained regarding the effect of layup parameters and interference value on maximum assembly force, failure torque, and failure condition in CFRP-metal interference fit joints. The concluding remarks of the study are as follows:

(1) Keeping the interference value at 0.1 mm: the larger the layup angle, the higher the maximum assembly force and failure torque of the interference fit joints. However, excessive angle of layup has a relatively insignificant improvement on maximum assembly force and failure torque, and excessive angle layup increases the failure index of the CFRP shaft tube and the metal shaft head. The effects of layup angle are more apparent on maximum assembly force and failure torque than layup sequence. For the CFRP shaft tube layup, set the small-angle layup in the middle and the large angle layup on the outside, the smaller the failure index, the higher the safety performance.

(2) If the layup parameters are kept at $[\pm 75^{\circ}]$: the maximum assembly force and failure torque of interference fit joints are roughly linearly related to the value of interference. The higher the interference value, the higher the maximum assembly force and failure torque of the interference fit joints. However, the failure index of the interference fit joints also increases with the amount of interference value. Five interference values of 0.02, 0.04, 0.06, 0.08, and 0.1 mm are applied to the interference fit joints, the stress values on the contact surfaces are all at extreme values at the beginning of the assembly and then increase with the displacement of the assembly.

Other factors, such as electrochemical corrosion, are expected to also influence the performance of CFRP-metal interference fit joints, although these are not investigated in this study. Opportunities exist to further improve the structural properties. This shortcoming can be complemented in follow-up studies.

Nomenclature

- d diameter
- radial variations
- Е Young's modulus
- coefficient of friction
- F maximum assembly
- h laminate thickness
- l interference length
- Μ failure torque
- N number of layers
- S flat depth
- radius
- и displacement
- Poisson's ratio
- σ stress
- ε strain
- radial interference value

Subscripts

- contact surface С
- f **CFRP**

- inner
- metal
- outer
- radial, circumferential and axial directions r,θ

Funding information: This research was funded by the National Natural Science Foundation of China (Grant Nos. 51975435, 51879209, and 51775400) and the National Key Research and Development Program (Grant No. 2018YFB1501200).

Author contributions: I would like to thank all those authors who helped me to concise my paper. Jinguang Zhang, who put forward many valuable suggestions for my paper. Huang Yang and Xiangyu Ma have made great contributions in experiments and simulations. Other authors give a lot of help in experiments and translation.

Conflict of interest: Authors state no conflict of interest.

References

- [1] Yao CX, Qi ZC, Chen WL, Zhang CQ. Effect of CF/PEEK plasticity behavior on the mechanical performance of interference-fit joint. Polym Compos. 2021;42(5):2574-88.
- Inverarity SB, Das R, Mouritz AP. Composite-to-metal joining using interference fit micropins. Compos Part A: Appl Sci Manuf. 2022;156:106895.
- Seung WL, Dai GL. Composite hybrid valve lifter for automotive engines. Compos Struct. 2004;71(1):26-33.
- Sang-Young K, Dave K. Interference-fit effect on improving bearing strength and fatigue life in a pin-loaded woven carbon fiber-reinforced plastic laminate. J Eng Mater Technol. 2019;141(2):1-7.
- Li J, Zhang KF, Li Y, Liu P, Xia JJ. Influence of interference-fit size on bearing fatigue response of single-lap carbon fiber reinforced polymer/Ti alloy bolted joints. Tribol Int. 2015 Aug;93:151-62.
- Wang XY, Lou ZF, Wang XD, Xu CL. A new analytical method for press-fit curve prediction of interference fitting parts. J Mater Process Tech. 2017;250:16-24.
- Mucha J. Finite element modeling and simulating of thermomechanic stress in thermocompression bondings. Mater Des. 2009;30(4):1174-82.
- Manuel P, Naoufel N, Marc S. Study of an interference fit fastener assembly by finite element modelling, analysis and experiment. Int J Interact Des Manuf. 2012;6(3):171-7.
- Strozzi A, Baldini A, Giacopini M, Bertocchi E, Bertocchi L. Normalization of the stress concentrations at the rounded edges of a shaft-hub interference fit. J Strain Anal Eng Des. 2011;46(6):478-91.
- [10] Sun Y, Hu WP, Shen F, Meng QC, Xu YM. Numerical simulations of the fatigue damage evolution at a fastener hole treated by

- cold expansion or with interference fit pin. Int J Mech Sci. 2016:107:88-200.
- [11] Bi YB, Jiang JF, Ke YL. Effect of interference fit size on local stress in single lap bolted joints. Adv Mech Eng. 2015;7(6):54-6.
- [12] Taghizadeh H, Chakherlou TN, Ghorbani H, Mohammadpour A. Prediction of fatigue life in cold expanded fastener holes subjected to bolt tightening in Al alloy 7075-T6 plate. Int J Mech Ences. 2014;90:6-15.
- [13] Oswald FB, Zaretsky EV, Poplawski JV. Interference-fit life factors for ball bearings. Tribol Trans. 2010;54(1):1-20.
- [14] Dario C, Massimiliano DA, Nicolò V. Design and optimization of shaft-hub hybrid joints for lightweight structures: analytical definition of normalizing parameters. Int J Mech Ences. 2012;56(1):7-85.
- [15] Hu JS, Zhang KF, Xu YW, Cheng H, Xu GH, et al. Modeling on bearing behavior and damage evolution of single-lap bolted composite interference-fit joints. Compos Struct. 2019;212:452-64.
- [16] Hu JS, Zhang KF, Yang QD, Cheng H, Liu P, et al. An experimental study on mechanical response of single-lap bolted CFRP composite interference-fit joints. Compos Struct. 2018;196:76–88.
- [17] Chao L, Zhang KF, Li XG, Li Y. A method for predicting the onset and expanding of the damage during CFRP interference-fit joining process. Adv Mater Res. 1938;2012:166–9.
- [18] Binnur GK. Effect of the clearance and interference-fit on failure of the pin-loaded composites. Mater Des. 2009;31(1):85-93.
- [19] Sang-Young K, Bin H, Dave (Dae-Wook) K, Chun SS, Ha CS. Bearing strength of interference-fit pin joined glass fiber reinforced plastic composites. J Compos Mater. 2020;54(12):1579-91.

- [20] Liu P, Zhang KF, Li Y. Experiment study on interference amount of rivet joining for CFRP/Al components. Appl Mech Mater. 2013;2728:127–31.
- [21] Song DL, Li Y, Zhang KF, Cheng H, Liu P, et al. Micromechanical analysis for microscopic damage initiation in fiber/epoxy composite during interference-fit pin installation. Mater Des. 2015;89:36-49.
- [22] Wu T, Zhang KF, Cheng H, Liu P, Song DL, et al. Analytical modeling for stress distribution around interference fit holes on pinned composite plates under tensile load. Compos Part B Eng. 2016;100:176–85.
- [23] Karthik PR, Kobye B, Gyu-Hyeong L. Larry lessard improving load sharing in hybrid bonded/bolted composite joints using an interference-fit bolt. Compos Struct. 2016;149:329–38.
- [24] Liu HW. Mechanics of material. 6th edn. Beijing: Higher Education Press; 2017.
- [25] Shuge L, Zhangtao H, Pengju Z. Study on the design method of interference fit between gear and shaft of automobile transmission. J Phys: Conf Ser. 2021;1885(5). doi: 10.1088/1742-6596/1885/5/052067.
- [26] Gibson RF. Principles of composite material mechanics. Boca Raton, FL: CRC Press; 2016.
- [27] Hu JS, Zhang KF, Yang QD, Cheng H, Liu SN, et al. Fretting behaviors of interface between CFRP and coated titanium alloy in composite interference-fit joints under service condition. Mater Des. 2017;134(15):91–102.
- [28] Giacomo C, Paul MW, Felice R, Angelo M, Roberto C. Lay-up optimization of laminated composites using a modified branch and bound method. Open Mech Eng J. 2018;12(1):138-50.
- [29] Giacomo C, Stuart A, Felice R, Angelo M, Roberto C, Weaver PM. Realistic stacking sequence optimization of an aero-engine fan blade-like structure subjected to frequency. Deforma Manuf Constraints Open Mech Eng J. 2018;12(1):151-63.